D. V. Brockway, University of Illinois Report No. COO-1195-197, 1970 (unpublished).
[27]Illinois-Genova-Hamburg-Milano-Saclay-Harvard-Toronto-Wisconsin Collaboration, Phys. Rev. Letters 26, 929 (1971).
[28]Aachen-Berlin-Bonn-CERN-Cracow-Heidelberg-London-Vienna Collaboration, Phys. Letters 34B, 160 (1971).
[29]V. G. Lind *et al.*, Nucl. Phys. B14, 1 (1969).

PHYSICAL REVIEW D VOLUME 5, NUMBER 3 1 FEBRUARY 1972

Coincidence Experiment on Inelastic Electron-Proton Scattering in the Region of the $\Delta(1236)$ at $q^2 = -0.35$ and -1.0 (GeV/c)^2

S. Galster, G. Hartwig, H. Klein, J. Moritz,
K. H. Schmidt, W. Schmidt-Parzefall, and D. Wegener
Institut für Experimentelle Kernphysik der Universität (TH) und des Kernforschungszentrums Karlsruhe, Karlsruhe, Germany

and

J. Bleckwenn
Deutsches Elektronen-Synchrotron (DESY) Hamburg, Germany
(Received 31 August 1971)

We present measurements on inelastic electron-proton scattering in the region of the $\Delta(1236)$ resonance for two values of q^2. A fit to the single-arm and the π^0-electroproduction cross sections gave a separation of the resonance and the nonresonant background contribution. The transition form factor $G_M^*(q^2)$ was determined and shown to have a different dependence on q^2 than the magnetic nucleon form factor, confirming earlier measurements. A fit to the angular dependence of the π^0-electroproduction cross section gives some indications that smaller multipole amplitudes contribute to the resonance besides the dominating M_{1+} amplitude.

INTRODUCTION

The scattering of high-energy electrons on protons provides information about the structure of the proton and its excited states. Experimentally this information can be extracted from the energy spectrum of electrons scattered off hydrogen at a fixed angle. In the case of single-pion electroproduction additional information can be collected through measurements where the outgoing proton or pion is detected in coincidence with the scattered electron. This permits a separation of the two electroproduction processes $e+p \to e+p+\pi^0$ and $e+p \to e+n+\pi^+$ and leads to the determination of angular dependences. Thus differential cross sections are obtained which can be compared with theories describing the structure of the proton and its excited states.

In this paper we report on an investigation of the structure of the first nucleon resonance $\Delta(1236)$ which was performed at the Deutsches Elektronen-Synchrotron (DESY) at Hamburg. High-energy electrons were extracted from the synchrotron and focused on a liquid-hydrogen target. Scattered electrons as well as coincident protons were detected.

The experimental setup and detection apparatus is described in some detail in Sec. I. The procedure followed for evaluation of the measured data is described in Sec. II and results are given and interpreted in Sec. III.

I. EXPERIMENTAL SETUP

The experiment was performed at the Deutsches Elektronen-Synchrotron (DESY) at Hamburg.[1] A schematic drawing of the apparatus is shown in Fig. 1. A slowly extracted beam of high-energy electrons was focused on a liquid-hydrogen target of 3-cm diameter. The intensity of the beam was measured in a secondary-emission monitor and a totally absorbing Faraday cup which stopped the beam.

The spectrometer for detection of scattered electrons was mounted on a platform pivoting horizontally around the target and consisted of a collimator, a bending magnet, four digitized wire spark chambers with ferrite-core readout, and scintillation counters including a shower counter. Whenever a coincidence signal arrived from the scintil-

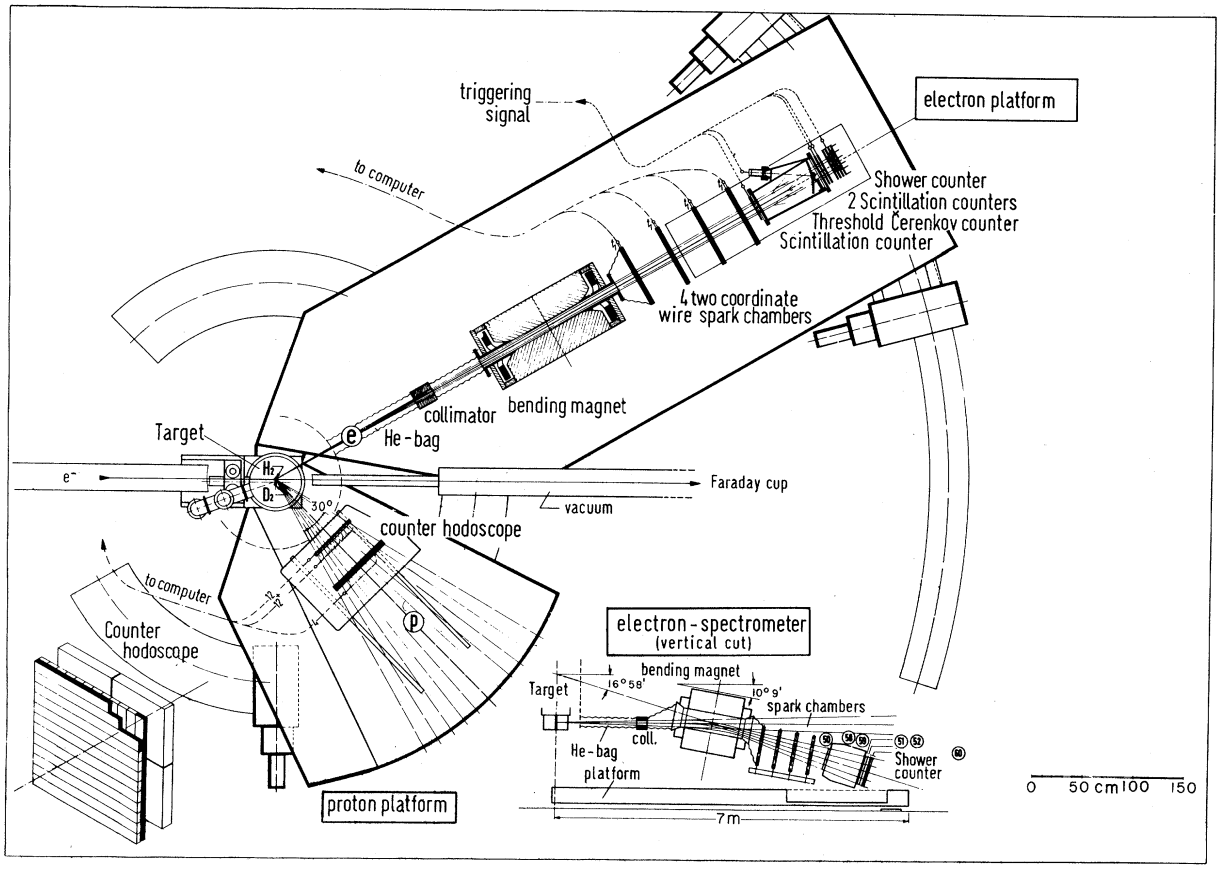

FIG. 1. Experimental setup for e-p scattering.

lation counters a high-voltage pulse was applied to the spark chambers, leading to the formation of sparks at those points where the triggering particle had traversed the chambers. A second independent spectrometer also pivoting horizontally around the target was used for detection of charged particles coincident with scattered electrons. It consisted of 12 horizontal and 12 vertical scintillation counters which formed a hodoscope of 12-by-12 elements subtending a large solid angle around the direction of the virtual photon emitted in the scattering process. For spectrometer details see Table I.

All data pertaining to an individual scattering event, such as x and y coordinates of the sparks, coincidence signals from scintillation counters, scaler contents, and results of analog-to-digital conversion were read in to an on-line computer each time the electron spectrometer had registered the traversal of a particle. No thresholds were applied at this time to make sure that no bias was introduced during the measurements.

The events were transferred to disk storage and were accessible at any time for simple on-line computations like construction of histograms and for display programs. Both types of programs had previously been stored on disk and were activated at the user's demand. At the end of a run all event data were transferred to magnetic tape.

Some problems like track finding and computation of the scattered particle's energy were solved for most of the events during the data-taking process. Final evaluation of the data was performed off line.

II. EVALUATION OF THE DATA

Measurements were made for two different values of the momentum transfer squared, defined as

$$q^2 = (p_1 - p_3)^2 = -4E_1E_3 \sin^2(\tfrac{1}{2}\theta),$$

where p_1 and p_3 are the 4-vectors of the incoming and outgoing electron, $p = (E, \vec{p})$, and a metric is used where $a \cdot b = a_0 b_0 - \vec{a} \cdot \vec{b}$. See Fig. 2 for a definition of parameters.

The kinematical parameters chosen for the two measurements are given in Table II.

In both settings of the electron spectrometer the

TABLE I. Details of the instrumentation.

Spectrometer details		
Beam dimensions at the target	horizontal (FWHM)	3 mm
	vertical	1 mm
Diameter of the target		15 or 30 mm
Electron spectrometer		
Angular range		12–90 deg
Angular acceptance	horizontal	1.57 deg
	vertical	1.41 deg
Solid angle		0.68 msr
Four digitized wire spark chambers with ferrite-core readout behind a bending magnet with homogeneous field		
Three scintillation counters	Nos. 50, 51, 52	
One gas-Čerenkov counter	Nos. 58, 59	
One shower counter	No. 60	
Momentum resolution	measured ±0.6%	
Momentum acceptance	measured ±20%	
Proton detector		
Angular range		25–90 deg
Angular acceptance	horizontal	30 deg
	vertical	30 deg
Solid angle		260 msr
12 horizontal scintillation counters	Nos. 1–12	
12 vertical scintillation counters (length, width, thickness 432, 36, 10 mm)	Nos. 13–24	
2×2 "dE/dx" counters (length, width, thickness 216, 216, 50 mm)	Nos. 25, 26, 27, 28	
Scintillation material Nuclear Enterprise NE 102A		
Fast electronic equipment Chronetics		

elastic peak and the first resonance could be observed simultaneously.

The second spectrometer then showed protons from elastic scattering which were used for the calculation of the efficiency of that detector, and a major fraction of the protons from the decay of pion-nucleon states in the region of the first resonance.

For definition of an electron scattering event the following criteria were used. At least three of the four wire spark chambers must have given spark coordinates such that a mathematical straight line could be fitted to them within given deviations. If this particle trajectory could be traced back through the homogeneous field of the bending magnet and through the opening of the collimator into the target, it was assumed to be an electron trajectory. To test this assumption a pulse-height spectrum of the shower-counter signals of these events was formed from the raw event data. It showed a clean shower peak with negligible contamination outside the peak. The remaining 10% of the events taken were lacking sufficient information to find a single-particle trajectory or showed a track which could not be traced back to the target. The pulse-height spectrum of shower-counter signals of these events showed no structure except a bump at the position of the expected shower peak. This fraction of about 1% of the data was later included in the absolute cross-section values. The knowledge of the scattered electron's trajectory through the spark chambers permitted the evaluation of the scattering angle and scattering plane of each individual event. This knowledge was used to correct the influence of the finite collimator opening.

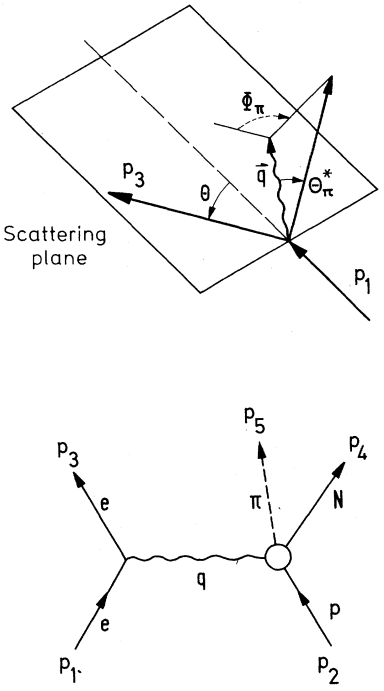

FIG. 2. Definition of kinematical variables, scattering diagram.

An energy spectrum obtained is shown in Fig. 3.

TABLE II. Kinematical parameters.

Primary energy E_1	Scattering angle θ	4-momentum transfer squared q^2 [(GeV/c)^2]
2.7 GeV	14°	−0.35 at W=1236 MeV
3.2 GeV	21°	−1.0 at W=1236 MeV

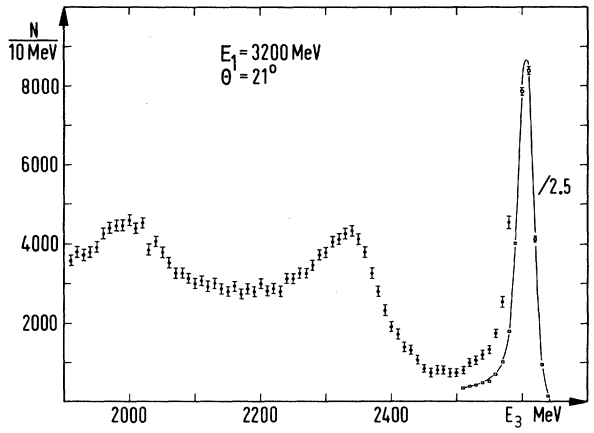

FIG. 3. An energy spectrum for e-p scattering.

Together with the elastic peak the first and part of the second nucleon resonance show up clearly.

After subtraction of the elastic scattering peak and its radiative tail, radiative corrections were applied to the inelastic continuum according to a prescription of Mo and Tsai,[2] using cross-section predictions given by Gutbrod and Simon.[3] Thus measured cross sections for electroproduction of pions in the region of the $\Delta(1236)$ resonance were obtained.

The same technique was applied to electron spectra formed from scattering events where a coincident proton had been detected. This led to cross sections for single-π^0 electroproduction. Subtracting these from the "single-arm" cross sections – where the scattered electron only was detected – we obtained cross sections for single-π^+ electroproduction.

Scattering events where a coincident proton was detected were used to extract detailed information about angular dependences for π^0 electroproduction. In the one-photon-exchange approximation the cross section can be written as

$$\frac{1}{\Gamma_t}\frac{d^3\sigma}{d\Omega_e dE_3 d\Omega_\pi^*}=\frac{d\sigma_v}{d\Omega_\pi^*}(W, q^2, \epsilon, \Theta_\pi^*, \Phi_\pi),$$

where $d\sigma_v/d\Omega_\pi^*$ is the photoproduction cross section for virtual photons with $q^2 \neq 0$. W is the invariant mass of the outgoing πN system. Γ_t, ϵ, Θ_π^*, and Φ_π are defined as usual.[4] (See also Fig. 2.)

This cross section is made up of several parts with different angular dependences. These are contributions from virtual-photon polarization states and their interference terms,[4]

$$\frac{d\sigma}{d\Omega_\pi}=A+\epsilon B+\epsilon C\sin^2\Theta_\pi^*\cos(2\Phi_\pi)+[\epsilon(\epsilon+1)]^{1/2}D\sin\Theta_\pi^*\cos\Phi_\pi .$$

Here A and B are cross-section terms due to unpolarized transverse and longitudinal photons, and C and D represent transverse polarization and an interference between transverse and longitudinal photons, respectively. The latter two contributions can be distinguished by their characteristic Φ_π dependence.

Since the polarization parameter ϵ was not varied in our measurements for a single value of q^2, the terms A and B in the cross section could not be separated and in our calculations were represented by a single term $\bar{A}=A+\epsilon B$.

For the fits to the measured cross sections s and p waves only were considered which then give rise to the following coefficients:

$$\bar{A}=\bar{A}_0+\bar{A}_1\cos\Theta_\pi^*+\bar{A}_2\cos^2\Theta_\pi^*,$$

$$C=C_0,$$

$$D=D_0+D_1\cos\Theta_\pi^*.$$

Of these the two coefficients $\bar{A}_1$ and D_1 could not be determined since coincident protons were detected without separation between backward and forward emission in the c.m. system. The $\cos\Theta_\pi^*$ term connected with $\bar{A}_1$ and D_1 then excluded their determination.

III. RESULTS

Elastic Cross Sections

Together with the inelastic cross sections the elastic peak was measured and the cross section for elastic scattering evaluated. They are given in Table III together with predictions according to the assumed validity of the Rosenbluth formula,

TABLE III. Cross sections for elastic electron-proton scattering.

E_1 (MeV)	θ	q^2 [(GeV/c)^2]	Cross sections (μb/sr) Measured	Rosenbluth dipole-fit scaling law	Prediction Berger *et al.*
2700	14°	−0.400	0.7805 ± 0.0234	0.8361	0.795
3200	21°	−1.105	0.023 65 ± 0.000 69	0.023 07	0.023 53

TABLE IV. Cross sections for electroproduction of pions. The errors contain a systematic and normalization error of 3%. $E_1 = 2700$ MeV, $\theta = 14°$, $q^2(1236) = -0.35$ (GeV/c)^2, $\epsilon(1236) = 0.95$.

E_3 (MeV)	K (MeV)	W (MeV)	$\frac{1}{\Gamma_t}\frac{d^2\sigma}{d\Omega_e dE_3}$ (μb)		
			$e+p \to e+\begin{cases} p+\pi^\circ \\ n+\pi^+ \end{cases}$	$e+p \to e+p+\pi^\circ$	$e+p \to e+n+\pi^+$
2330	171	1096	25.9 ± 10		
2320	182	1105	46.9 ± 10	9.5 ± 9	37.4 ± 14
2310	193	1114	70.9 ± 10	23.7 ± 10	47.2 ± 14
2300	203	1123	76.1 ± 10	33.2 ± 10	42.9 ± 14
2290	214	1132	107.2 ± 11	42.7 ± 10	64.5 ± 15
2280	225	1141	123.0 ± 11	52.2 ± 10	70.8 ± 15
2270	236	1150	159.9 ± 11	73.6 ± 10	86.3 ± 15
2260	247	1159	208.8 ± 12	97.2 ± 10	111.6 ± 16
2250	258	1168	252.8 ± 13	111.4 ± 10	141.4 ± 16
2240	269	1177	313.1 ± 14	142.2 ± 11	170.9 ± 17
2230	280	1185	353.8 ± 14	187.4 ± 11	166.4 ± 17
2220	291	1194	396.9 ± 15	209.8 ± 12	187.1 ± 19
2210	301	1202	452.9 ± 16	249.0 ± 13	203.9 ± 20
2200	313	1211	469.7 ± 17	249.0 ± 13	220.7 ± 21
2190	323	1219	487.4 ± 18	278.5 ± 13	208.9 ± 22
2180	334	1227	478.8 ± 17	276.1 ± 13	202.7 ± 21
2170	345	1236	431.4 ± 16	250.0 ± 13	181.4 ± 20
2160	356	1244	395.0 ± 15	243.0 ± 13	152.0 ± 19
2150	367	1252	369.1 ± 14	231.2 ± 13	137.9 ± 19
2140	377	1260	327.5 ± 14	207.5 ± 12	120.0 ± 18
2130	388	1268	289.2 ± 14	183.8 ± 12	105.4 ± 18
2120	399	1276	266.7 ± 13	154.1 ± 11	112.6 ± 17
2110	410	1284	218.8 ± 12	138.5 ± 11	80.3 ± 16
2100	421	1292	192.0 ± 12	128.0 ± 11	64.0 ± 16
2090	432	1300	199.7 ± 12		
2080	442	1307	182.4 ± 12		
2070	453	1315	171.9 ± 11		
2060	463	1323	159.4 ± 11		
2050	475	1331	153.7 ± 11		
2040	487	1339	146.0 ± 11		
2030	497	1346	139.3 ± 10		
2020	508	1354	132.6 ± 10		
2010	518	1361	132.1 ± 10		
2000	530	1369	134.5 ± 10		

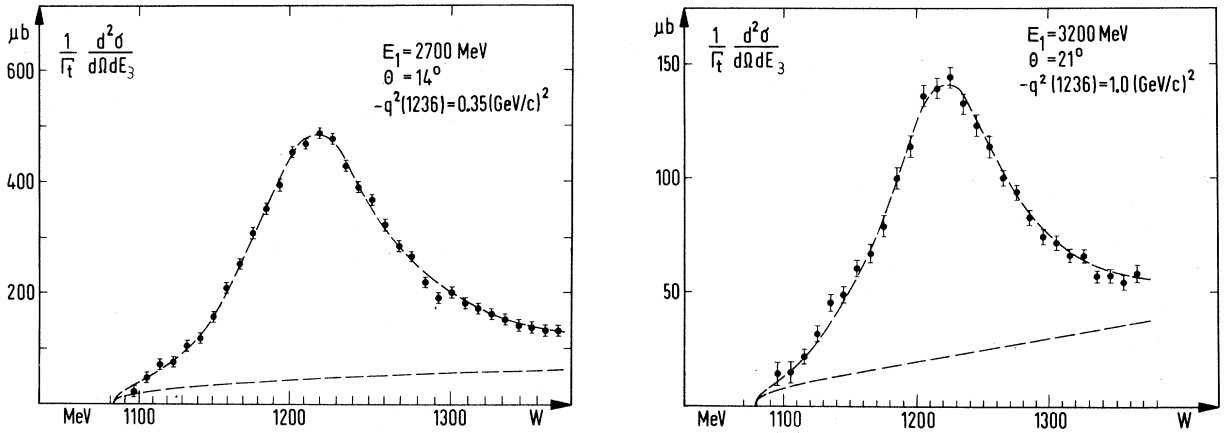

FIG. 4. Cross section $(1/\Gamma_t)d^2\sigma/d\Omega dE_3$ for inelastic scattering in the region of the $\Delta(1236)$ resonance. The curves represent the phenomenological fit through the total cross sections and the fitted nonresonant background.

TABLE V. Cross sections for electroproduction of pions. The errors contain a systematic and normalization error of 3%. $E_1=3200$ MeV, $\theta=21°$, $q^2(1236)=-1.0$ (GeV/c)^2, $\epsilon(1236)=0.89$.

E_3 (MeV)	K (MeV)	W (MeV)	$\frac{1}{\Gamma_t}\frac{d^2\sigma}{d\Omega_e dE_3}$ (μb) $e+p\to e+\begin{cases}p+\pi^0\\ n+\pi^+\end{cases}$	$e+p\to e+p+\pi^0$	$e+p\to e+n+\pi^+$
2470	171	1096	15.2±3	1.5±1.5	13.7±6
2460	183	1106	16.3±3	5.4±5	10.9±6
2450	195	1116	22.2±3	13.0±5	9.2±6
2440	208	1127	32.7±3	15.3±5	17.4±6
2430	220	1137	45.5±3	19.1±5	26.4±6
2420	232	1147	49.0±3	27.5±5	21.5±6
2410	246	1157	60.1±4	29.8±5	30.3±6
2400	257	1167	67.7±4	35.2±5	32.5±6
2390	269	1177	79.4±4	42.9±5	36.5±6
2380	281	1186	100.4±4	53.9±6	46.5±7
2370	293	1196	114.4±4	63.9±6	50.5±7
2360	306	1206	136.5±5	80.7±6	55.8±8
2350	318	1215	140.0±5	81.5±6	58.5±8
2340	331	1225	144.7±5	86.4±7	58.3±9
2330	343	1234	133.0±5	90.2±7	42.8±9
2320	355	1243	123.7±5	70.0±7	53.7±9
2310	367	1252	114.4±4	76.5±6	37.9±7
2300	380	1262	101.5±4	57.0±6	44.5±7
2290	392	1271	94.5±4	57.0±6	37.5±7
2280	404	1280	82.9±3	47.4±5	35.5±6
2270	417	1289	74.7±3	44.7±5	30.0±6
2260	429	1298	72.3±3	44.7±5	27.6±6
2250	440	1306	66.5±3	37.1±5	29.4±6
2240	453	1315	66.5±3	39.3±5	27.2±6
2230	465	1324	57.2±3	36.0±5	21.2±6
2220	478	1333	57.2±3	38.2±5	19.0±6
2210	490	1341	53.7±3	30.6±5	23.1±6
2200	502	1350	58.3±3	45.9±5	12.4±6

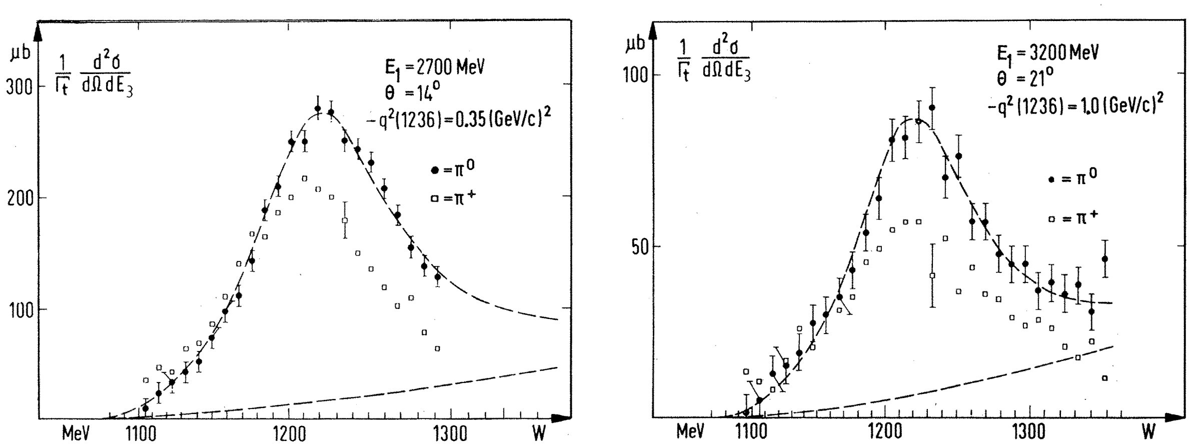

FIG. 5. Same as Fig. 4, except the $p\pi^0$ and $n\pi^+$ channels are separated.

the dipole fit, and the scaling law. In the last column of Table III not the dipole fit but a four-pole fit by Berger *et al.*[5] was used for the predictions. These latter values agree well with our measured cross sections.

Inelastic Cross Sections

The inelastic cross sections for single-pion electroproduction are listed in Tables IV and V and are shown in Figs. 4 and 5 together with curves fitted to the data. Three separate contributions were considered[6]:

(1) A relativistic Breit-Wigner resonance curve, neglecting G_E^* and G_C^*,

$$\sigma_{\rm res}=\frac{\pi\alpha\vec{q}^2}{2KWM}\frac{\Gamma(W)}{(W-W_{\rm res})^2+\frac{1}{4}\Gamma^2(W)}G_M^{*2}(q^2) \qquad (1)$$

for excitation of the $\Delta(1236)$ resonance with the width of the resonance[7]

$$\Gamma(W)=\frac{0.128(0.85|\vec{p}_\pi^*|/m_\pi)^3}{1+(0.85|\vec{p}_\pi^*|/m_\pi)^2} \quad \text{(measured in GeV)}.$$

(2) A nonresonant background polynomial

$$\sigma_{\rm nres}=(W-W_{\rm th})^{1/2}\sum_{n=0}^{N}a_n(q^2)(W-W_{\rm th})^n$$

with the square root $(W-W_{\rm th})^{1/2}$ giving the correct threshold behavior.

(3) A small contribution

$$\sigma_{1520}=\frac{b(q^2)\Gamma(1520)}{(W-1520)^2+\frac{1}{4}\Gamma^2(1520)}$$

from the $N(1520)$ resonance.

Numerical data about the fits can be found in Table VI. From these data and the curves plotted in Figs. 4 and 5 it can be seen that a consistent fit to all measured cross sections was obtained with the above formulas. The correct result of the ratio 2:1 for the excitation of the $\Delta_{3/2,3/2}$ resonance in the π^0 and the π^+ channel was reproduced, giving support to the separation procedure.

The fit for the nonresonant background at threshold is significantly different in the two single-pion electroproduction channels. This can be explained by the Kroll-Ruderman theorem which – in effect – states that close to the threshold for photoproduction only the cross section for π^+ production is different from zero and proportional to the square root $(W-W_{\rm th})^{1/2}$.

The $\gamma N\Delta$ transition form factor $G_M^*(q^2)$ for magnetic dipole excitation, as obtained from Eq. (1) in the fits to the measured cross sections, is listed in Table VI. A plot of this form factor divided by the magnetic nucleon form factor, together with other available data,[6,8] is shown in Fig. 6 as a function of q^2. This plot demonstrates that $G_M^*(q^2)$ falls off faster with q^2 than the magnetic nucleon form factor.

Fits to the measured proton distributions were performed with free parameters $\bar{A}_0$, $\bar{A}_2$, C_0, and D_0. The differential cross sections in the center-of-mass system of the outgoing hadrons were transformed into counting rates on the proton hodoscope elements and fitted to the measured counting rates by the method of least squares. A 20-MeV bin size was used.

TABLE VI. Measured values of $G_M^*(q^2)$ and relative contributions of $\sigma_{\rm res}$, $\sigma_{\rm nres}$, and σ_{1520} to total cross sections.

Outgoing hadrons	q^2 [(GeV/c)^2]	$G_M^*(q^2)$	$\sigma_{\rm res}$	$\sigma_{\rm nres}$	σ_{1520}
				In polynomial	
$p\pi^0+n\pi^+$	−0.35	1.324 ±3.5%		only $a_0\neq 0$	$b=0$
			W(MeV) = 1100, 50%	50%	
			1220, 90%	10%	
			1300, 72%	28%	
$p\pi^0$	−0.35	1.274 ±4%		only $a_1\neq 0$	$b=0$
			W(MeV) = 1100, 90%	10%	
			1220, 93%	7%	
			1300, 75%	25%	
$p\pi^0+n\pi^+$	−1.0	0.4307 ±3.5%		only $a_0\neq 0$	
			W(MeV) = 1100, 40%	60%	0%
			1220, 84%	15%	1%
			1300, 63%	32%	5%
$p\pi^0$	−1.0	0.4307 ±5%		only $a_1\neq 0$	
			W(MeV) = 1100, 90%	10%	0%
			1220, 92%	6%	2%
			1300, 64%	28%	8%

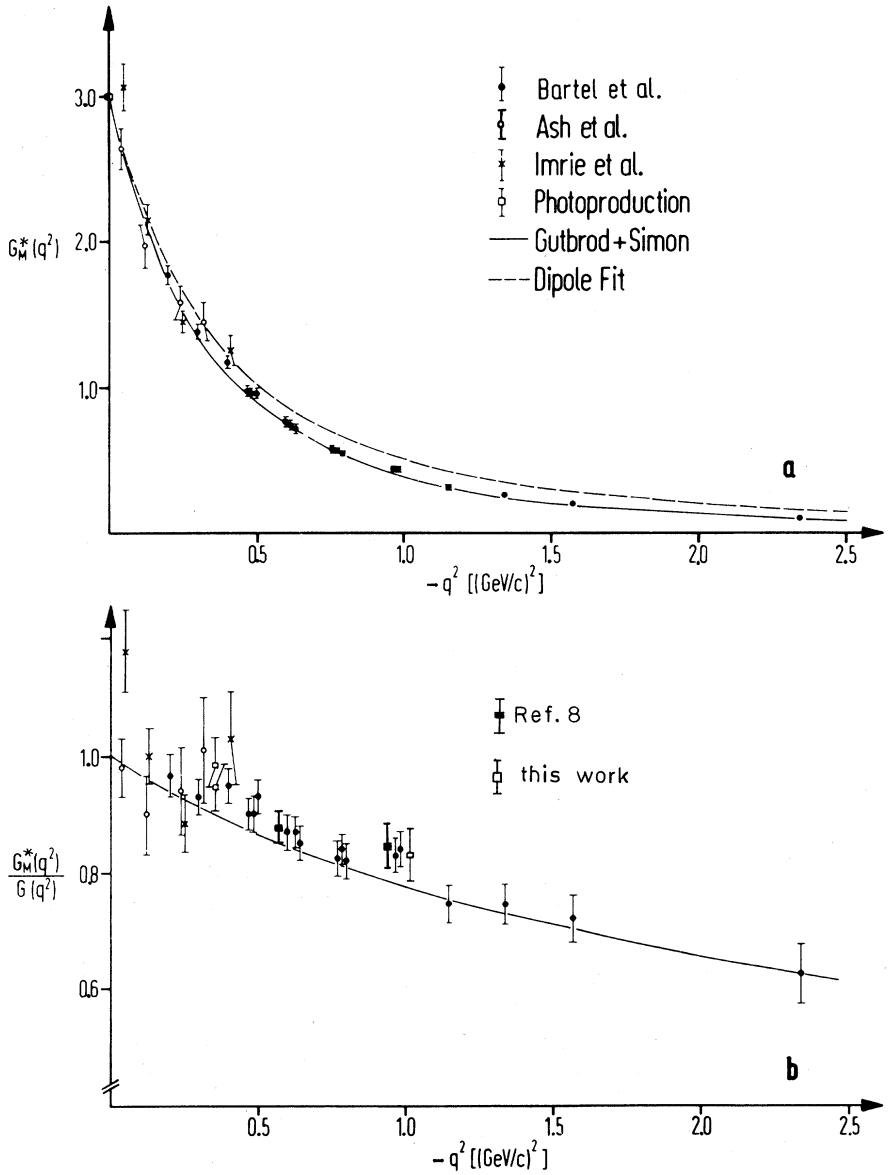

FIG. 6. A plot of the transition form factor $G_M^*(q^2)$ as a function of q^2 in two different representations. This figure was adapted from Ref. 6.

The results for $q^2 = -1.0$ (GeV/c)^2 derived from the fits are listed in Table VII. A fit to our data at $q^2 = -0.35$ (GeV/c)^2 was finally abandoned because the information about angular dependences of the cross sections was insufficient at that q^2 value.

Several aspects show up clearly for $q^2 = -1.0$ (GeV/c)^2. The terms $\bar{A}_0$, $\bar{A}_2$, and C_0 show a clear resonance structure which is expected from the dominating magnetic dipole amplitude M_{1+} for the excitation of the $\Delta(1236)$ resonance. The magnitude of the interference term D_0 – connected with an angular dependence $\sin\Theta_\pi^* \cos\Phi_\pi$ – turns out to be so small that it is below the level of detection in our measurements. Therefore only an upper limit is given, relative to the dominating term $\bar{A}_0$. The ratio of the cross sections $\bar{A}_0 : \bar{A}_2 : C_0$ should be $-\frac{5}{3} : 1 : 1$ assuming that only the M_{1+} amplitude contributes and that the E_{1+} and S_{1+} amplitude can be neglected. Our measurements differ slightly from this numerical relationship which indicates that other amplitudes contribute to the cross section.

For our measurements at $q^2 = -1.0$ (GeV/c)^2 a fit was made regarding only those terms in the cross sections $\bar{A}_0$, $\bar{A}_2$, and C_0 that contained the M_{1+} amplitude. As a result it turns out that the ratio $E_{1+}/M_{1+} = -0.048 \pm 0.021$ near the maximum

TABLE VII. Electroproduction of neutral pions $e+p \rightarrow e+p+\pi^0$. $E_1=3200$ MeV, $\theta=21°$, $q^2=-1.0$ (GeV/c)^2, $\epsilon(1236)=0.89$.

E_3 (MeV)	K (MeV)	W (MeV)	Cross sections (μb/sr) $\bar{A}_0$	$-\bar{A}_2$	$-C_0$	D_0	χ^2 per deg of freedom
			±10%	±20%	±20%	$\lvert D_0\rvert<0.1\,\bar{A}_0$	
2400	257	1167					
2390	269	1177	4.0	1.8	0.7		0.73
2380	281	1186					
2370	293	1196	6.3	3.6	1.9		1.04
2360	306	1206					
2350	318	1215	8.4	5.8	3.1		1.05
2340	331	1225					
2330	343	1234	8.9	5.1	3.9		0.84
2320	355	1243					
2310	367	1252	7.3	3.7	2.2		0.93
2300	380	1262					
2290	392	1271	5.2	1.9	2.1		1.41
2280	404	1280					
2270	417	1289	4.0	1.3	0.7		
2260	429	1298					

of the resonance.

These results may be compared with measurements of Mistretta *et al.*,[9] the DESY-Collège de France collaboration,[8] and of Hellings *et al.* at Daresbury NPL.[10] There is good agreement between our measurements and the published data.

ACKNOWLEDGMENTS

This work was supported by the Bundesministerium für Bildung und Wissenschaft.

We wish to thank Professor A. Citron, Professor H. Schopper, Professor W. Jentschke, Professor E. Lohrmann, Professor M. W. Teucher, and Professor G. Weber for their constant interest in this experiment. Further thanks are due to the synchrotron group, the floor-service group, and all the technical groups at DESY for their excellent help. The wholehearted support of Ing. H. Sindt and P. Adler in constructing, testing, and carrying out the experiment is gratefully acknowledged.

[1]Details are given in J. Moritz, DESY Report No. DESY F23-71/1 (unpublished).

[2]L. W. Mo and Y. S. Tsai, Rev. Mod. Phys. 41, 205 (1969).

[3]F. Gutbrod and D. Simon, Nuovo Cimento 51A, 602 (1967); F. Gutbrod, DESY Reports No. DESY 69/22 (unpublished) and No. DESY 69/33 (unpublished).

[4]C. W. Akerlof, W. W. Ash, K. Berkelman, and M. Tigner, Phys. Rev. Letters 14, 1036 (1965).

[5]Ch. Berger, V. Burkert, G. Knop, B. Langenbeck, and K. Rith, University of Bonn Report No. 1-075, 1969 (unpublished).

[6]W. Bartel, B. Dudelzak, H. Krehbiel, J. McElroy, U. Meyer-Berkhout, W. Schmidt, V. Walther, and G. Weber, Phys. Letters 28B, 148 (1968); W. Bartel, DESY Report No. DESY F22-69/3 (unpublished).

[7]R. H. Dalitz and D. G. Sutherland, Phys. Rev. 146, 1180 (1966).

[8]W. Albrecht, F. W. Brasse, H. Dorner, W. Flauger, K. H. Frank, J. Gayler, V. Korbel, J. May, P. D. Zimmerman, A. Courau, A. Diaczek, J. C. Dumas, G. Tristram, J. Valentin, C. Aubret, E. Chazelas, and E. Ganssauge, Nucl. Phys. B25, 1 (1970); W. Albrecht, F. W. Brasse, H. Dorner, W. Fehrenbach, W. Flauger, K. H. Frank, J. Gayler, V. Korbel, J. May, P. D. Zimmerman, A. Courau, A. Diaczek, J. C. Dumas, G. Tristram, J. Valentin, C. Aubret, E. Chazelas, and E. Ganssauge, *ibid.* B27, 615 (1971); J. Gayler, DESY Report No. DESY F21-71/2 (unpublished).

[9]C. Mistretta, J. A. Appel, R. J. Budnitz, L. Carroll, J. Chen, J. R. Dunning, M. Goitein, K. Hanson, D. C. Imrie, and R. Wilson, Phys. Rev. 184, 1487 (1969).

[10]R. D. Hellings, J. Allison, A. B. Clegg, F. Foster, G. Hughes, P. Kummer, R. Siddle, B. Dickinson, M. Ibbotson, R. Lawson, H. E. Montgomery, W. J. Shuttleworth, A. Sofair, and J. Fannon, Nucl. Phys. B32, 179 (1971).